Progress in Organic Coatings 78 (2015) 188–199

Contents lists available at ScienceDirect

Progress in Organic Coatings

journal homepage: www.elsevier.com/locate/porgcoat

Synthesis of POSS-containing fluorosilicone block copolymers via RAFT polymerization for application as non-wetting coating materials

Bo Li [a], Xiaohui Li [a], Kaiqiang Zhang [a], Hui Li [b], Yunhui Zhao [a], Lixia Ren [a], Xiaoyan Yuan [a,*]

[a] School of Materials Science and Engineering, and Tianjin Key Laboratory of Composite and Functional Materials, Tianjin University, Tianjin 300072, China
[b] School of Chemistry and Chemical Engineering, Shandong Key Laboratory of Fluorine Chemistry and Chemical Engineering Materials, University of Jinan, Jinan 250022, China

ARTICLE INFO

Article history:
Received 22 February 2014
Received in revised form 3 September 2014
Accepted 5 September 2014
Available online 20 September 2014

Keywords:
RAFT polymerization
Block copolymer
POSS
PDMS
Fluoropolymers
Surface properties

ABSTRACT

By using a polydimethylsiloxane (PDMS) macro-chain transfer agent with trithiocarbonate groups at both ends, fluorosilicone block copolymers containing polyhedral oligomeric silsesquioxane (POSS) were synthesized via reversible addition–fragmentation chain transfer (RAFT) polymerization. Acryloisobutyl POSS (APOSS) and 2,2,3,4,4,4-hexafluorobutyl acrylate (HFBA) were sequentially introduced into the copolymers. The obtained triblock copolymers PDMS-*b*-$(PAPOSS)_2$ exhibited a low polydispersity index (PDI) of less than 1.42 in the first 6 h of polymerization, but the PDI value became broader later because of the steric hindrance of the POSS macromer. The POSS-containing fluorosilicone pentablock copolymers with a PDI of about 2.0, which were prepared by the further RAFT polymerization of HFBA, showed clear microphase separation. The average roughness values of the copolymer films were enhanced by introducing POSS, and a certain POSS content led to a significant decrease of the receding contact angle. Measurements of water contact angles and ice shear strengths demonstrated that the non-wetting properties of the copolymer films were improved by the incorporation of both POSS and fluorine blocks. The block copolymers combine the advantages of POSS, PDMS and fluoropolymers, and can be potentially applied as non-wetting coating materials for anti-icing or anti-frosting.

1. Introduction

Low surface energy materials have been widely used in the preparation of ice-phobic, anti-frosting surfaces, and non-wetting fabrics for decades, because their low dielectric constants contribute to the weakness of the electrostatic interactions at interfaces [1]. Due to the unique surface properties, low solubility and high thermal stability, polydimethylsiloxane (PDMS) has been extensively employed with other polymeric components to generate novel coating materials, especially those with well-defined architectures, such as block and graft copolymers [2–5]. Moreover, fluoropolymers are attractive in coating applications due to their excellent properties of weather resistance and chemical stability. Therefore, much work has been done to incorporate fluorinated polymeric components into PDMS block copolymers to obtain well-defined fluorosilicone-containing copolymers [4,5]. By combination of the advantages of fluoropolymers and silicone, the fluorosilicone copolymers could satisfy requirements for the uses in the extreme conditions such as at the ultralow temperatures.

Polyhedral oligomeric silsesquioxanes (POSS) comprises hybrid organic–inorganic frameworks with silicon–oxygen cubic core functionalized with organic groups at the apex of each silicon atom [6]. The physical properties and chemical stability of the copolymers can be improved by the addition of POSS via free radical polymerization [7,8], living anionic polymerization [9,10], and atom transfer radical polymerization (ATRP) [11–13]. In addition, reversible addition–fragmentation chain transfer (RAFT) polymerization is also an effective method for the production of complex polymer architectures [2,14–22], and the versatility makes RAFT polymerization a promising choice for embedding sterically hindered POSS macromers into copolymers [16–20].

A methacrylate-functionalized cubic silsesquioxane homopolymer (PMAPOSS) was first synthesized by using *S*-1-dodecyl-*S*′-(α,α′-dimethyl-α″-acetic acid) trithiocarbonate (DDMAT) as the RAFT agent [16]. The RAFT polymerization of the MAPOSS macromer at 100 or 200 of [MAPOSS]/[DDMAT] molar ratio produced broad polydispersities (1.3–1.6) due to the presence of low molecular weight species that were promoted by the chain termination reaction [16]. A tadpole-shaped organic/inorganic hybrid

* Corresponding author. Tel.: +86 22 8740 1870; fax: +86 22 8740 1870.
E-mail addresses: yuanxy@tju.edu.cn, xyuan28@yahoo.com (X. Yuan).

http://dx.doi.org/10.1016/j.porgcoat.2014.09.004
0300-9440/

POSS-poly(acrylic acid) (POSS-PAA) polymer was prepared by hydrolysis of POSS-poly(*tert*-butyl acrylate) that was synthesized via RAFT polymerization in a living manner using a POSS-containing trithiocarbonate chain transfer agent (CTA) [17]. Ramirez and co-workers synthesized fluoroalkyl methacrylate-POSS copolymer with methyl methacrylate (MMA) via RAFT polymerization [18]. At a feed percentage of the fluoroalkyl methacrylate macromer FMA-POSS to MMA in the range 0–25 wt%, they failed to acquire the homopolymer PFMAPOSS, but a well-controlled P(FMAPOSS-*co*-MMA) copolymer with lower polydispersity index (1.03–1.08) was obtained [18]. Additionally, they found that the non-wetting properties of the copolymer were enhanced with the increased FPOSS content according to dynamic contact angle measurements [18]. Deng and co-workers successfully synthesized well-defined hybrid PMAPOSS-*b*-PMMA block copolymers with different POSS block lengths using cumyl dithiobenzoate as the RAFT agent, and these POSS-based block copolymers were further applied as modifiers of epoxy thermosets [19]. PMAPOSS-*b*-PAA and PMAPOSS-*b*-P(AA-*co*-St) were also synthesized via the RAFT polymerization, and the effects of styrene (St) block length and content on the block copolymer morphologies in water were investigated [20]. As the block chain became longer, the micelle structure of the copolymer switched sequentially from dispersed-spheres to onion-like, and ultimately to hierarchical onion-clusters [20].

In our previous study, a series of polyacrylate-*b*-PDMS and polyacrylate-*g*-PDMS copolymers with three different molecular weights of PDMS blocks or side chains were studied for the formation of hydrophobic anti-icing surfaces [8], but the effect of POSS was not investigated in detail. In this study, we attempted to synthesize POSS-containing fluorosilicone block copolymers via RAFT polymerization that are also aimed at non-wetting applications. According to the selection principles of RAFT agents and monomers described in the reference [21], trithiocarbonate DDMAT was used to couple with PDMS, and the obtained macro-chain transfer agent CTA-PDMS-CTA with trithiocarbonate groups at both ends was employed to mediate the RAFT polymerization of acryloisobutyl POSS (APOSS) and 2,2,3,4,4,4-hexafluorobutyl acrylate (HFBA). Different from our previous report on polyacrylate-PDMS copolymers [8], it was assumed that the prepared POSS-containing ABA triblock or fluorosilicone CABAC pentablock copolymers could integrate the advantages of low surface energy possessed by PDMS and poly(fluoroalkyl acrylate), and that the incorporation of APOSS could modify the topological surfaces of the copolymer films. Low surface energy surfaces with microphase structures for potential applications as hydrophobic coating materials for anti-icing or anti-frosting would be expected to obtain.

2. Experimental methods

2.1. Materials

α,ω-Dihyhroxy-terminated poly(dimethylsiloxane) (HO-PDMS-OH, 2000 g/mol) was supplied by Hangzhou Silong Chem-Tech, Hangzhou, China. APOSS was purchased from Hybrid Plastics, USA, and used as received. 2,2,3,4,4,4-Hexafluorobutyl acrylate (HFBA) was supplied by Xeogia Fluorin-Silicon Chemical Co. Ltd., China, and purified by passing it though a neutral alumina column prior to use. 2-Hydroxyethyl acrylate (HEA) was purchased from Sinopharm Chemical Reagent Co. Ltd., China, and also passed though alumina before use [22]. 2,2′-Azobisisobutyronitrile (AIBN) was obtained from Tianjin Kemiou Chemical Reagent Co. Ltd., China, and used after recrystallization by ethanol. α,α,α-Trifluorotoluene (TFT) was purchased from Tianjin Heowns Biochem Technologies LLC, Tianjin, China. The RAFT agent DDMAT was synthesized in our laboratory according to a procedure described previously [23]. All other reagents were supplied by Tianjin Kermel Reagent Co. Ltd., China, and used without further purification.

2.2. Synthesis

The synthesis process of the PDMS macro-RAFT agent contained two main steps [22]. As shown in Scheme 1, DDMAT was first converted into acyl chloride by reaction with oxalyl chloride and then reacted with HO-PDMS-OH to produce CTA-PDMS-CTA.

The synthesized CTA-PDMS-CTA was used as the macromolecular chain transfer agent to synthesize a PDMS-*b*-$(PAPOSS)_2$ triblock copolymer via RAFT polymerization (Scheme 1). Typically, CTA-PDMS-CTA (0.12 g, 0.06 mmol), APOSS (1.12 g, 1.2 mmol), AIBN (2.0 mg, 0.012 mmol) and toluene (0.75 mL) were charged to a 50 mL round-bottom flask with a magnetic stir bar followed by bubbling with nitrogen for 30 min to remove residual oxygen and moisture. The bottle was subsequently placed in a water bath at 70 °C for 24 h and stirred under nitrogen atmosphere. For kinetic analysis, a certain amount of the reactant was withdrawn at predetermined time intervals and analyzed by ^{1}H nuclear magnetic resonance (^{1}H NMR) and gel permeation chromatography (GPC) without purification. After polymerization proceeded for 24 h, the reaction mixture was precipitated in an excess amount of methanol. The product designated as S1 was then dried in a vacuum oven overnight at 40 °C for further uses.

The obtained PDMS-*b*-$(PAPOSS)_2$ triblock copolymer was then used as the macro-CTA for synthesis of PDMS-*b*-[PAPOSS-*b*-PHFBA-*b*-P(HFBA-*co*-HEA)]$_2$ pentablock copolymers via RAFT polymerization. In order to cast a polymer film, a small amount of HEA was added as potential crosslinking units. Typically, PDMS-*b*-$(PAPOSS)_2$ (0.9 g, 0.1 mmol), HFBA (2.36 g, 10 mmol), AIBN (2.0 mg, 0.01 mmol), and toluene (0.75 mL) were added to a 50 mL round-bottom flask having a magnetic stir bar followed by purging of the mixture with nitrogen for 30 min to remove residual oxygen and moisture. The bottle was subsequently placed in water bath at 70 °C for 7 h under a nitrogen atmosphere. Then, HEA (0.23 g, 2 mmol) was introduced into the reaction bottle by a syringe, and the polymerization was maintained for a further 4 h. Finally, the polymerization was terminated by diluting the reaction system with THF and immersing the bottle in liquid nitrogen. To purify the product, the synthesized viscous liquid was precipitated in an excess amount of ethanol, and then dried in a vacuum oven overnight at 40 °C. Two compositions of the POSS-containing fluorosilicone acrylate pentablock copolymers were prepared with 30:1 and 100:1 ratios of $[HFBA]_0/[macro\text{-}CTA]_0$ and designated as S2 and S3, respectively (Table 1).

For comparison, PDMS-*b*-[PHFBA-*b*-P(HFBA-*co*-HEA)]$_2$ triblock copolymer was also synthesized by using the PDMS macro-RAFT agent CTA-PDMS-CTA via RAFT polymerization. As an example, CTA-PDMS-CTA (0.12 g, 0.06 mmol), HFBA (1.42 g, 6 mmol), and AIBN (2.0 mg, 0.012 mmol) were reacted for 24 h at 70 °C as described above. For kinetic analysis, certain amounts of the reactant were withdrawn at predetermined time intervals. Then, HEA (0.14 g, 1.2 mmol) was introduced into the reaction bottle using a syringe and the polymerization was allowed to continue for another 4 h. After reaction, the reaction mixture was precipitated in an excess amount of methanol. The product designated as S4 was then dried in a vacuum oven overnight at 40 °C (Table 1).

2.3. Characterizations

^{1}H NMR spectra were obtained on an INOVA 500 MHz spectrometer using $CDCl_3$ as solvent. The GPC measurement was performed with tetrahydrofuran (THF) as eluent at 40 °C and a flow rate of 1 mL/min with a Waters 1515 Isocratic HPLC pump equipped with

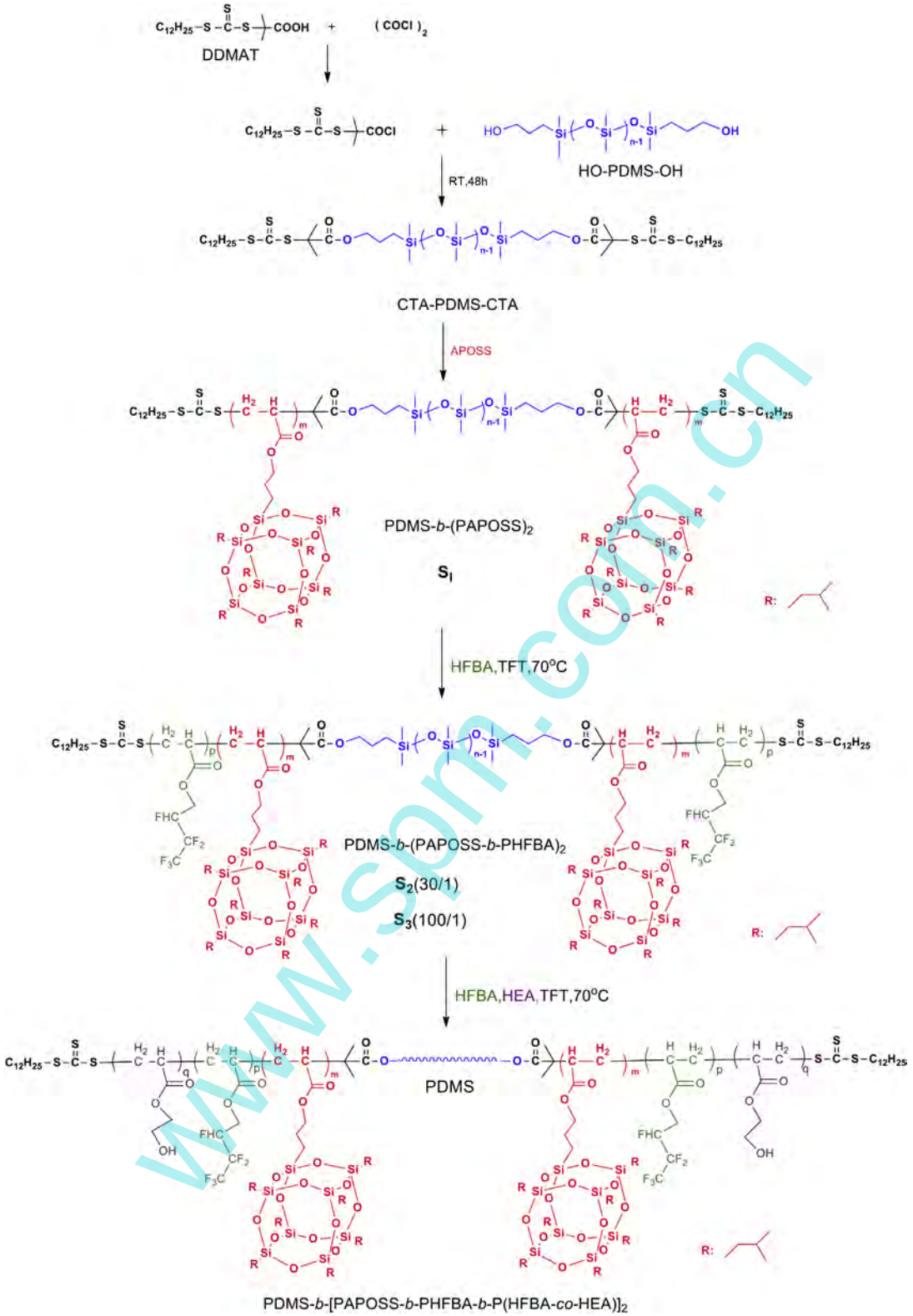

Scheme 1. Synthesis of POSS-containing fluorosilicone block copolymers via RAFT polymerization. PDMS-*b*-(PAPOSS)$_2$ is designed as S1, and PDMS-*b*-[PAPOSS-*b*-PHFBA-*b*-P(HFBA-*co*-HEA)]$_2$ as S2 and S3 in different monomer feeding ratios. S4 is referred to PDMS-*b*-[PHFBA-*b*-P(HFBA-*co*-HEA)]$_2$ for comparison.

a Waters 2414 refractive index detector. Monodisperse polystyrene standards were used for calibration. Fourier transform infrared spectra (FTIR) were recorded in a Perkin-Elmer Spectrum 100 spectrometer. Polymer films were cast on KBr pellets from TFT.

Differential scanning calorimetric (DSC) analysis were carried out in a NETZSCH DSC 200 F3 differential scanning calorimeter (Germany), and the samples were heated from −150 °C to 220 °C at a heating rate of 10 °C/min under a dry nitrogen atmosphere.

Table 1
Composition of the POSS-containing fluorosilicone copolymers and their molecular weights.

Sample [a]	Structure	$[HFBA]_0/[macro\text{-}CTA]_0$ [a]	f_{PDMS} (wt%) [b]	f_{POSS} (wt%) [b]	f_{HFBA} (wt%) [b]	$\overline{M}_n$ (kDa) [c]	PDI
–	CTA-PDMS-CTA	–	100	–	–	2.81	1.21
–	PAPOSS	–	–	100	–	–	–
S1	PDMS-*b*-$(PAPOSS)_2$	–	30.0	70.0	–	8.57	1.30
S2	PDMS-*b*-[PAPOSS-*b*-PHFBA-*b*-P(HFBA-*co*-HEA)]$_2$	30	18.6	43.2	38.2	13.88	2.10
S3	PDMS-*b*-[PAPOSS-*b*-PHFBA-*b*-P(HFBA-*co*-HEA)]$_2$	100	11.1	25.7	63.2	23.32	2.00
S4	PDMS-*b*-[PHFBA-*b*-P(HFBA-*co*-HEA)]$_2$	100	9.5	–	90.5	26.94	1.04

[a] The macro-CTA represents the PDMS-*b*-$(PAPOSS)_2$ macro-chain transfer agent for both S2 and S3, and CTA-PDMS-CTA for S4, respectively.
[b] f_{PDMS}, f_{POSS} and f_{HFBA} are the weight percentage of PDMS, APOSS and HFBA blocks in the synthesized copolymers, respectively calculated from the molecular weights.
[c] The $\overline{M}_n$ values were obtained from GPC measurement for CTA-PDMS-CTA and S1, and from ^1H NMR results for S2, S3 and S4.

Transmission electron microscope (TEM) images were recorded in a JEOL JEM100CXII transmission electron microscope operated at 100 kV. A droplet of each copolymer solutions (1 wt% in TFT) was deposited on a carbon-coated copper grid. After a few seconds, excess solution was removed by blotting with filter paper. Staining was performed with ruthenium tetroxide (RuO_4) vapor for 2 h to increase the contrast between the PDMS, APOSS and polyacrylate domains. Scanning electron microscope (SEM) images were recorded on a TENSOR machine. The SEM samples were prepared by spinning the solutions of the block copolymers (10 wt% in TFT) onto flat aluminum foils, which were then dried at 130 °C for 3 h.

X-ray diffraction (XRD) patterns were recorded in a D/max 2500 machine using a wavelength $\lambda = 0.154$ nm and a scattering angle $2\theta = 3–50°$. The patterns were then azimuthally integrated to get the corresponding XRD intensity profiles as functions of the scattering angle.

Surface composition was investigated using X-ray photoelectron spectroscopy (XPS) with a Perkin-Elmer PHI 5000C ECSA X-ray photoelectron spectrometer under an ultra-high vacuum less than 5×10^{-8} Torr at 45° with Al K radiation (1486.6 eV) operating at 24.2 W. The tested area was a circle of 100 μm diameter.

Atomic force microscope (AFM) images were obtained in tapping mode from a CSPM5500A microscope of Benyuan Nano-Instruments equipped with an E-type vertically engaged piezoelectric scanner. The AFM samples were prepared by dip-coating the solutions of block copolymers (10 wt% in TFT) onto freshly cleaved silicon wafer surfaces, and then dried at 130 °C for 3 h.

Static contact angles, advancing angles and receding angles were measured on a JC2000D contact angle meter from Shanghai Zhongchen Equipment Ltd., China. A droplet of distilled water (5 μL) was placed on the sample surface and then expanded or shrunk at a flow rate in the range 0.1–1.0 μL/s via a syringe needle. Images of the droplets were captured by a CCD camera and analyzed to obtain the advancing and receding contact angles, and values of the water contact angle hysteresis were calculated [8]. The surface energies of the polymers were evaluated by measuring the static water and hexadecane contact angles on the surface [8]. All the presented contact angle values are averages of at least five or six measurements each.

Ice shear strengths of the block copolymers were measured in a custom humidity-controlled chamber in a low-humidity nitrogen atmosphere equipped with a force transducer (Model ZP-500, Imada, Japan) operated in push mode [24,25]. The push velocity was controlled at a constant rate of 0.5 mm/s by using a motion stage (Liansheng, Jianxi Province, China). Cylindrical glass columns with a common inner diameter of 10 mm were made by cutting glass tubes with well-polished ends and treating them with tridecafluoro-1,1,2,2-tetrahydrooctyl trichlorosilane for at least 24 h. A certain amount of water was filled in glass columns that were mounted on the samples held on the cooled plate. The temperature of the cooled plate was cooled at a rate of 2 °C/min to the target temperature and frozen at −15 °C for 3 h before the tests. The push force was recorded until the ice detached, and this force was used to calculate the ice shear strength ($n > 5$) by dividing the area (78.5 mm^2) between the ice and the coating surface.

The copolymer films were prepared by spraying the copolymer solutions in TFT at a concentration of 10 wt% on polished aluminum plates (20 mm × 20 mm); this allowed the solvent to evaporate completely at room temperature in air. A given amount of the curing agent (hexamethylene diisocyanate trimer) was added to each film. The prepared copolymer films were then annealed at 130 °C for 3 h and then characterized by SEM, XRD, XPS, AFM, contact angle, and ice shear strength measurements.

3. Results and discussion

The purpose of this study was to prepare low surface energy surfaces with hydrophobic microphase domains, which are beneficial for anti-icing, anti-frosting, and other non-wetting applications. As shown in Scheme 1, block copolymers were synthesized via RAFT polymerization of APOSSS and HFBA by using CTA-PDMS-CTA as the macro-chain transfer agent with both terminals coupled with DDMAT. A chain extension of the APOSS ("hard" block) from both ends of CTA-PDMS-CTA ("soft" block) was performed rather than the extension of a single end only, in order to highlight the important role of the POSS component in modifying the surface structure. Due to poor film-forming and low adhesive strength of APOSS and PDMS, HFBA and HEA units were incorporated to improve the polymer's physical properties and also to further enhance the hydrophobic properties of the final coatings. Here we examined two molar ratios of HFBA to the macro-chain transfer agent PDMS-*b*-$(PAPOSS)_2$, 30:1 and 100:1, to achieve different surface morphologies. It is expected that these POSS-containing fluorosilicone block copolymers can combine the advantages of PDMS and poly(fluoroalkyl acrylate), and that the incorporation of APOSS can modify the topological surfaces. Characterizations of the prepared copolymers were carried out to confirm the macromolecular structure, microphase separation structure, and the surface topology of the films.

3.1. Synthesis of the POSS-containing fluorosilicone block copolymers

The chemical structures of the typical copolymers were analyzed by FTIR and ^1H NMR as shown in Figs. 1 and 2, respectively. In the FTIR spectra of the copolymers (Fig. 1), the absorption peak in the range of 1000–1150 cm^{-1} was assigned to Si—O—Si asymmetric stretching vibrations that appeared in all the samples. In addition, the peak at 500 cm^{-1} detected in Fig. 1(b) and (c) was attributed to the Si—O—Si bending vibration, which is a characteristic signal of APOSS. The results also suggested that PDMS-*b*-$(PAPOSS)_2$ (sample S1) and pentablock copolymers PDMS-*b*-[PAPOSS-*b*-PHFBA-*b*-P(HFBA-*co*-HEA)]$_2$ (samples S2 and S3 with different monomer feeding ratios) contained PAPOSS moieties. Additionally, the appearance of a peak at 1750 cm^{-1} was due to

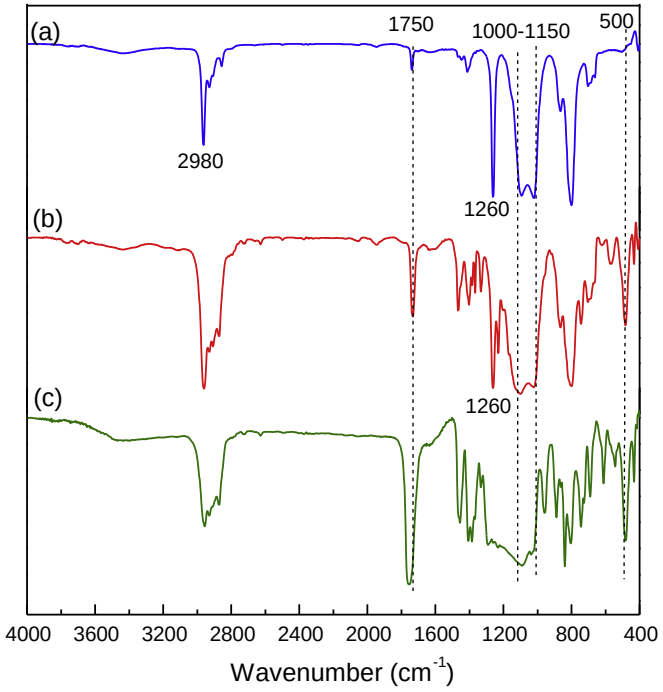

Fig. 1. FTIR spectra. (a) CTA-PDMS-CTA: 1000–1150 cm^{-1} (Si—O—Si stretching), 1260 cm^{-1} (Si—$(CH_3)_2$ flexing), 1750 cm^{-1} (—C=O stretching), and 2980 cm^{-1} (alkyl C—H stretching); (b) PDMS-*b*-$(PAPOSS)_2$: 500 cm^{-1} (Si—O—Si bending), 1000–1150 cm^{-1} (Si—O—Si stretching), 1750 cm^{-1} (—C=O stretching); (c) PDMS-*b*-[PAPOSS-*b*-PHFBA-*b*-P(HFBA-*co*-HEA)$]_2$: 500 cm^{-1} (Si—O—Si bending), 1000–1150 cm^{-1} (Si—O—Si stretching), 1750 cm^{-1} (—C=O stretching).

the existence of C=O stretching. Therefore, the gradual increase in the relative intensity of C=O stretching from Fig. 1(a) to (c) was attributed to the increased incorporation of APOSS and HFBA in the copolymers, both of which contain C=O groups.

^{1}H NMR was also used to confirm the structure of the copolymers as shown in Fig. 2. In the spectrum of CTA-PDMS-CTA [Fig. 2(a)], the resonance at 3.6 ppm, associated with —CH_2—OH in HO-PDMS-OH, has disappeared and there are two new signals at 3.2 ppm and 4.1 ppm attributed to the —CH_2—S— and —CH_2—O— groups, respectively. Moreover, the integral ratio of these two peaks was approximately 1:1, which indicated the —OH end groups essentially converted into the macro-chain transfer agent CTA-PDMS-CTA. With respect to PDMS-*b*-$(PAPOSS)_2$ [Fig. 2(b)], the signals at 0.1 ppm are contributed by the methyl protons of PDMS, and the resonance observed at 0.6 ppm is assigned to the methylene protons of PAPOSS. In addition, the methyl and methane protons of the isobutyl groups APOSS can be detected at 0.9 ppm and 1.9 ppm, respectively. The methylene protons from the PAPOSS blocks can be seen at 3.9 ppm, indicating that a successful chain extension reaction occurred [Fig. 2(b)]. In the ^{1}H NMR spectrum of PDMS-*b*-$(PAPOSS$-*b*-$PHFBA)_2$ [Fig. 2(c)], the resonances at 4.3–4.6 ppm and 4.8–5.1 ppm are associated with the protons of the —CH_2—CHF— and —CHF groups, respectively, suggesting that PDMS-*b*-$(PAPOSS$-*b*-$PHFBA)_2$ was synthesized successfully via RAFT polymerization.

GPC measurement was conducted to monitor the polymerization kinetics. The monomer conversion was evaluated using ^{1}H NMR spectra of the reactant withdrawn during the polymerization at predetermined time intervals (no shown in this paper), by comparing the peak area of methylene protons at —CH_2—CH_2—O—C(=O) (3.85 ppm) corresponding to PAPOSS and the peak area of the double bond signals (5.4 ppm) associated with the residual APOSS macromer. Fig. 3(a) showed that Ln($[M_0]/[M_t]$) increased linearly with the reaction time, suggesting that the monomer consumption followed the first order kinetics. Moreover, the molecular weight

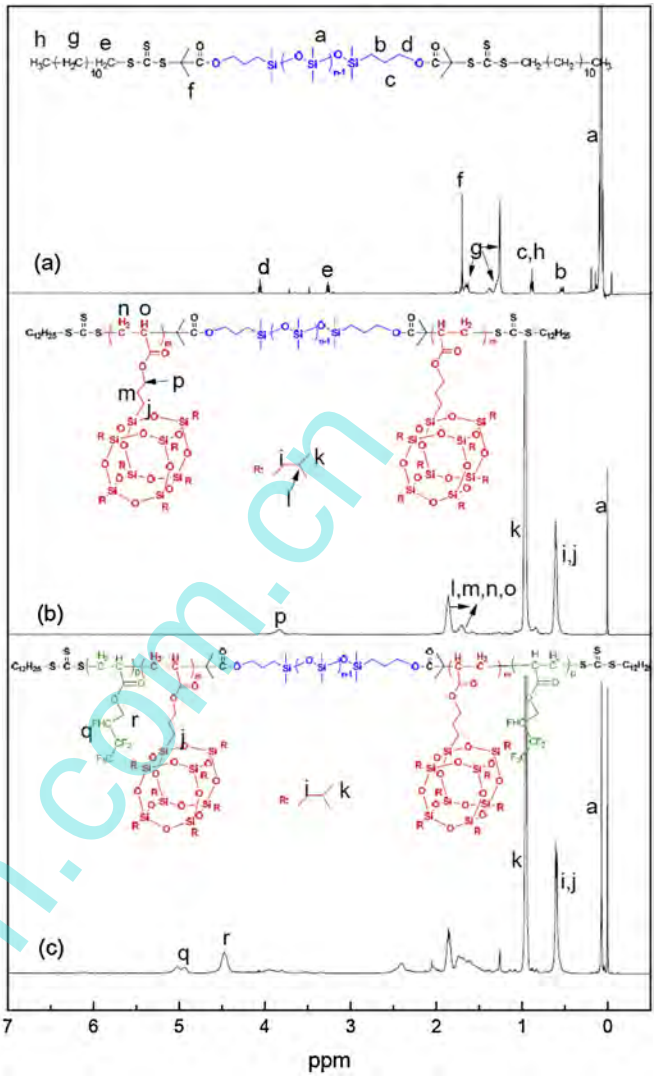

Fig. 2. ^{1}H NMR spectra. (a) CTA-PDMS-CTA: 0–0.1 [s, 6H, —Si(CH_3)$_2$], 0.6 [m, —Si—CH_2—], 0.8 [t, 3H, —$(CH_2)_8$—CH_3], 1.4 [—CH_2—$(CH_2)_8$—CH_3], 1.8 [s, 6H, —C(CH_3)$_2$—S—], 3.2 [t, 2H, —S—CH_2—$(CH_2)_8$—], and 4.2 [t, CH_2—CH_2—COO—]; (b) PDMS-*b*-$(PAPOSS)_2$: 0.91 [t, —SiCH_2CH(CH_3)$_2$], 1.6–1.95 [br, —CH_2CH(CH_3)$_2$ and —CH_2— or —CH— in the backbone], 3.85 [—OCOCH_2—]; (c) PDMS-*b*-(PAPOSS-*b*-PHFBA)$_2$: 0.91 [t, —SiCH_2CH(CH_3)$_2$], 1.1–2.2 [br, —CH_2CH(CH_3)$_2$ and —CH_2— or —CH— in the backbone], 3.85 [—OCOCH_2— in APOSS], 4.3–4.6 [—CH_2—CHF—], 4.8–5.1 [—CH_2—CHF—].

showed a linear relationship with the monomer conversion at the early stages of the polymerization with a polydispersity index (PDI) less than 1.3 [Fig. 3(b)]. At the beginning of the polymerization, it was assumed that the transfer of the CTA-PDMS-CTA between the propagating radical chains and dormant polymeric chains was instability, resulting in the slow growth of molecular weight with the increased conversion. Subsequently, efficient transfer between active and dormant chains ensured the extension of the PAPOSS chains and collisions were more likely to take place, so that the $\overline{M}_n$ value of the PAPOSS chains increased remarkably at moderate conversion (30–40%). However, in the later stages of the polymerization (after 6 h), a non-linear growth in the molecular weight of the copolymer was observed [Fig. 3(b)], indicating the RAFT polymerization has been lost control. The limited conversion of APOSS might be caused by the steric hindrance itself, that could possibly obstruct accession of the free radical chain to the terminal group of active polymeric chain, and reduce the probability of collisions among monomers, so that the molecular weight increased slowly

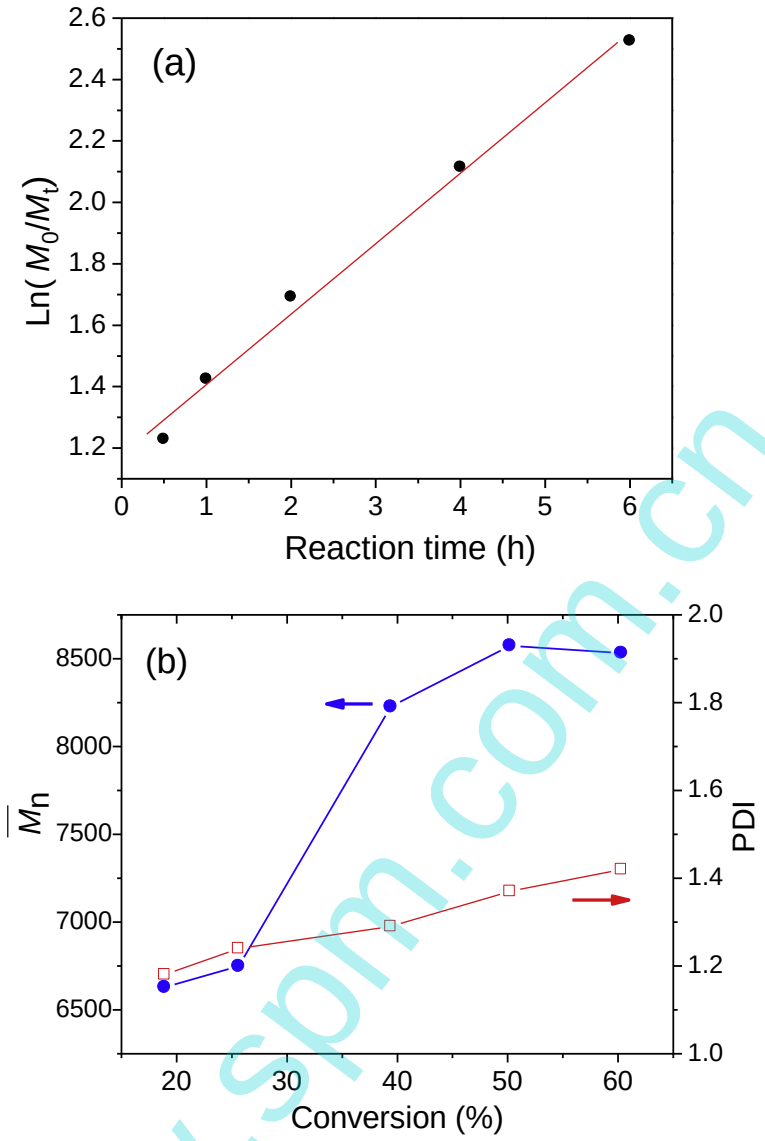

Fig. 3. Plot of Ln([M_0]/[M_t]) as a function of reaction time (a) and the dependence of molecular weight and polydispersity of PDMS-*b*-(PAPOSS)$_2$ on the monomer conversion (b).

to an asymptotic value. This phenomenon was also reflected in the GPC curves in Fig. 4. As the polymerization proceeds, a low molar mass shoulder appeared at longer polymerization time (6 h), because the macro-chain transfer agent of the triblock copolymer PDMS-*b*-(PAPOSS)$_2$ was feeble to mediate the polymerization of the APOSS macromer [19]. In the later stage of the polymerization, the steric effect as well as the increase of viscosity influenced the efficiency of chain transfer, and consequently the RAFT process was suppressed. Steric hindrance of the APOSS macromer and the increased viscosity of reactants may also be the reasons for the broadening of polydispersity (PDI = 1.18–1.42) shown in Fig. 3(b).

To investigate the transfer efficiency of CTA-PDMS-CTA and the controllability of the polymerization process, we also monitored the polymerization process of HFBA in the synthesis of PDMS-*b*-(PHFBA)$_2$ triblock copolymer (S4 in Table 1). The conversion of HFBA showed that the polymerization follows pseudo-first-order kinetics, and the PDI value remains in the range of 1.02–1.04, confirming a well-controlled polymerization of HFBA using CTA-PDMS-CTA as the RAFT agent.

The composition of the POSS-containing fluorosilicone copolymers in this study and the molecular weights were also summarized in Table 1. The triblock PDMS-*b*-(PAPOSS)$_2$ (S1) was obtained by introducing APOSS into the copolymers at each end of CTA-PDMS-CTA. Furthermore, the additional copolymerization with HFBA (as well as HEA for crosslinking) gave rise to two pentablock copolymers (S2 and S3) with different lengths of poly(fluoroalkyl acrylate) blocks. As shown in Table 1, the weight percentages of the POSS unit in the synthesized copolymers S2 and S3 were 43.2% and 25.7%, respectively, and S3 had two longer HFBA blocks with a weight percentage of 63.2%, which were higher than the corresponding block percentage in S2 of 38.2%. By contrast, S4 had a lower PDI of 1.04, and the S2 and S3 samples had broader PDI values of ca. 2 that were caused by the steric hindrance of the PDMS-*b*-(PAPOSS)$_2$ macro-RAFT agent.

3.2. Microphase separation

With different relative contents of PDMS, APOSS and HFBA, the prepared block copolymers would exhibit different structures. To make out the structure discrepancy, XRD patterns of S1, S2, S3, and S4 were collected, and the results were presented in Fig. 5. All samples were films cast from 10 wt% solutions of copolymers in TFT,

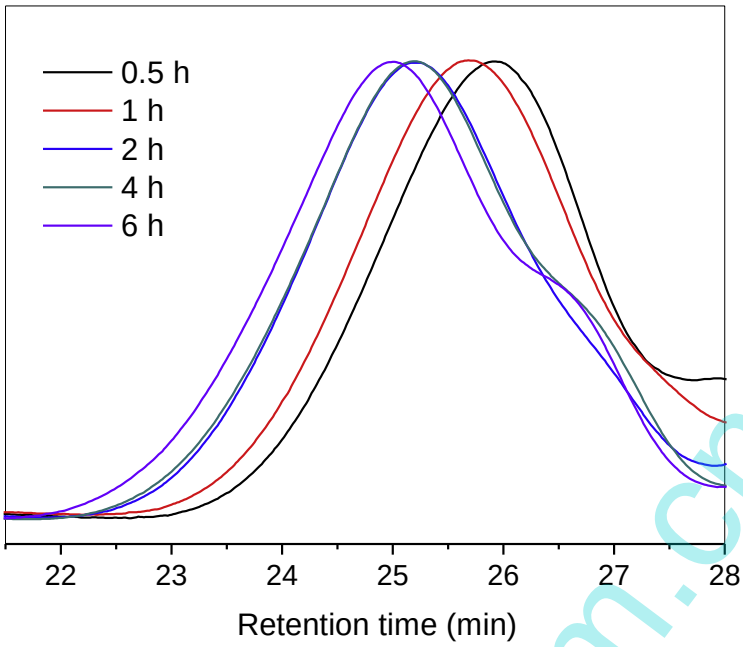

Fig. 4. Evolution of GPC curves of PDMS-*b*-(PAPOSS)$_2$.

and each of them was dried at 130 °C for 3 h. It could be seen that the XRD pattern for S1 has diffraction peaks at $2\theta = 8.3°$, 10.6°, and 18.6° that correspond to the diffraction pattern of the rhombohedral unit cell in the POSS structure. This meant that there were POSS crystals in sample S1, a result that agreed well with previous reports [26,27], showing that a related crystalline structure appeared in POSS-containing polymers or nanocomposites. In samples S2 and S3, it was found that the intensity of the two diffraction peaks at $2\theta = 8.3°$ and 18.6°, respectively, became weaker and relatively broad, and the intensity of the diffraction peak at $2\theta = 8.3°$ in S3 was also less than that in S2. It was suggested that the crystallization of POSS became less pronounced due to the decreased relative content of POSS (Table 2). A wide diffraction peak in the range $2\theta = 15°–30°$ for S4 was attributed to a polyacrylate bulk with no significant crystalline moieties.

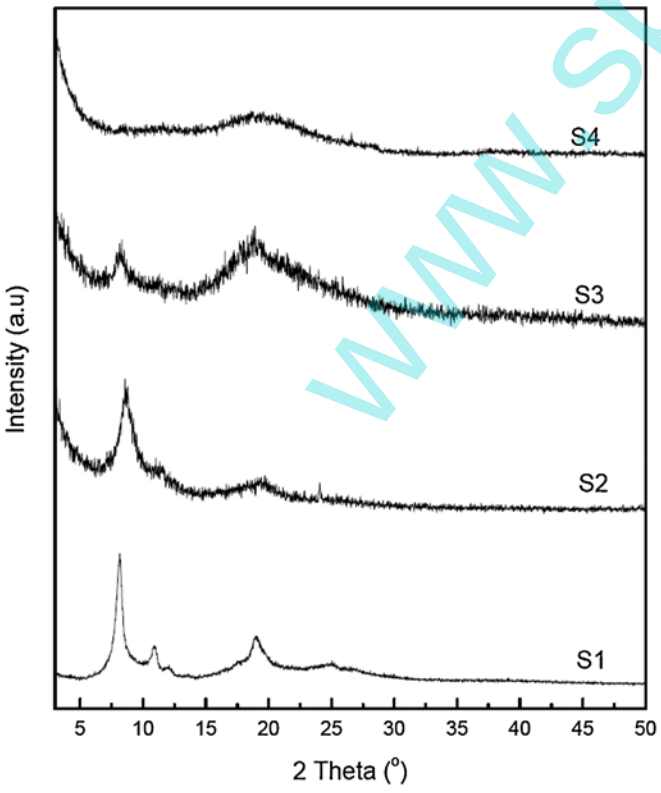

Fig. 5. XRD diffraction patterns of S1, S2, S3 and S4.

Fig. 6 showed DSC curves of the POSS-containing fluorosilicone block copolymers including PAPOSS, S1, S2, S3, and S4, and the corresponding values of glass-transition and melting temperatures were listed in Table 2. The homopolymer PAPOSS synthesized via RAFT polymerization mediated by using DDMAT was also shown for comparison, and PAPOSS had a glass transition temperature (T_{g3}) at 54.0 °C and an endothermic melting peak of POSS at 135 °C. In the DSC curve of PDMS-*b*-(PAPOSS)$_2$ (S1), the glass transition temperature T_{g3} of the PAPOSS block was 65.5 °C, and the endothermic peak at 127 °C could be attributed to the melting of PAPOSS crystals, which was also detected in the XRD measurement (Fig. 5). In addition, the glass transition temperature $T_{g1} = -117.4$ °C in the DSC curve of sample S1 could be associated with PDMS. It should be noted that T_{g1} of PDMS was not obvious in S1, which was presumably due to the relatively lower PDMS content in the copolymer S1 and the relatively restricted movement of the PAPOSS blocks. Similar results have been previously reported that the detection of T_{g1} in the DSC curves was related to the content of PDMS in the block copolymers [28,29]. Apart from S1, the T_{g3} values of POSS in S2 and S3 were 84.4 °C and 82.4 °C, respectively, with each about 20 °C higher than that of S1. This outcome was consistent with the result

Table 2
Thermal properties of the synthesized copolymers analyzed by DSC.[a]

Sample	T_{g1} (°C)	T_{g2} (°C)	T_{g3} (°C)	T_m (°C)
PAPOSS	–	–	54.0	135
S1	−117.4	–	65.5	122
S2	–	−8.8	79.5	106
S3	–	−10.5	81.0	96
S4	−123.0	−12.0	–	–

[a] T_{g1}, T_{g2} and T_{g3} are referred to the glass-transition temperatures of PDMS, PHFBA and PAPOSS block, respectively, and T_m is the melting temperature of the PAPOSS block.

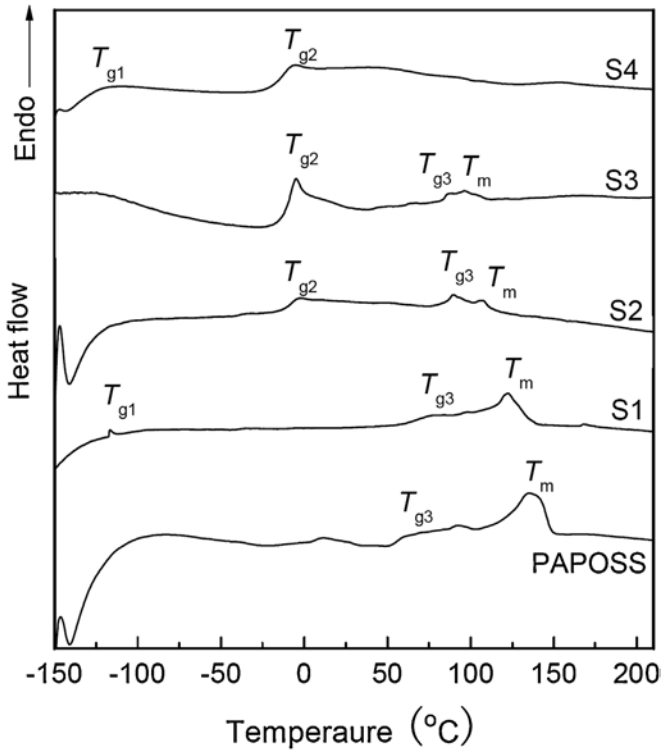

Fig. 6. DSC curves of PAPOSS, S1, S2, S3 and S4.

reported by Matyjaszewski and Mather that the glass transition temperature of PMAPOSS was about 20–25 °C lower than that for an ABA triblock copolymer [PMAPOSS-*b*-poly(*n*-butyl acrylate)-*b*-PMAPOSS] synthesized via ATRP bearing PMAPOSS repeating units [13]. The glass transition temperature of the PHFBA blocks, T_{g2}, was observed in the DSC curves of S2, S3, and S4, but the T_{g1} value of PDMS could not be detected because of a progressively lower PDMS content in these three copolymers (S2, S3, and S4). Two glass transition temperatures, T_{g1} (−123 °C) and T_{g2} (−12 °C), could be clearly viewed in S4 DSC curve, suggesting that there could be microphase separation occurring for this moiety.

The TEM measurement was further used to examine the microphase separation morphologies of the synthesized block copolymers. As shown in Fig. 7, it was difficult to distinguish the phases of PDMS and APOSS in S1 because of their similar Si—O structures. However, we could clearly observe obvious two-phase structures in S2, S3, and S4, an outcome that was consistent with the DSC results and suggested microphase separation happened in the copolymers. The PDMS and PAPOSS blocks have similar Si—O structures possessing higher electron densities compared with that of the PHFBA block, and the PDMS and PAPOSS domains appeared as dark regions, while PHFBA appeared as bright regions. There is no doubt that special POSS aggregation was generated because of the self-assembly of the block copolymers in TFT. It could be seen in S2 that the morphology evolves from a 'worm-like' to a 'sea-island' type with the increased HFBA content from 38.2% to 63.2% in the bulk structure (Table 1). In S3, the POSS domains possessed a quite polydispersity size (diameter from 100 to 200 nm). With the increase of the PHFBA block length, the interfacial free energy between the PDMS aggregate core and the solvent would increase [30]. To lower the free energy, the system was inclined to decrease the interfacial area by increasing the aggregate size and facilitating the aggregate fusion. Larger aggregate sizes (diameter larger than 200 nm) could be found in S4. This phenomenon was also found in the reference about self-assembly of PDMS-*b*-poly(2,2,3,3,4,4,4-heptafluorobutyl methacrylate) [30].

3.3. Surface properties

All the copolymers exhibited good solubility in TFT, even the PHFBA moieties, so that the copolymers were easily sprayed into films for surface characterizations. However, we were not able to analyze the sample S1 because it was too difficult to fix due to its hydrophobicity and its poor film-forming ability. In fact, the sample S1 was too fragile and easily fragmented.

The elemental compositions of the copolymer films were evaluated by XPS, and the characteristic data were shown in Table 3. Furthermore, strong characteristic signals of carbon, oxygen, silicon and fluorine were observed as expected. The characteristic signal intensity of fluorine increased significantly from 1.2% to 9.9% with increasing content of fluorine-containing groups in the copolymers S2, S3, and S4, whereas the characteristic signal intensity of silicon decreased slightly from 18.3% to 15.5%. It was also observed that the fluorine contents of S2, S3, and S4 detected on the air-side surfaces were lower in comparison with the weight percentage of the PHFBA block in the synthesized copolymers, i.e., 38.2%, 63.2% and 90.5%, which was likely due to the larger POSS groups hindering the movement of the fluorine groups toward the outside.

SEM images of S1, S2, S3 and S4 were shown in Fig. 8. The embedding of APOSS macromers contributed to an uneven film surface for S1. There were also wrinkle structures on the film surfaces of S2 and S3, which were thought to be the results of gradient crosslinking from surface to bulk, a phenomenon reported previously [31]. It is interesting to note that globular pits in the range of 200–300 nm appeared in the SEM image of S4, due to the different migration velocities of the PDMS and fluorine blocks to air during solvent annealing, as well as the block fractions of both components. Because of its lower surface energy compared with that of PDMS, the fluorine block migrated easier to the air-side during the drying process [2,32]. According to references, different aggregations could happen, showing layered, cylindrical, and spherical structures when the block length in a block copolymer changed [20,33,34]. The PDMS block in an "ABA" structured sample S4 was relatively short (f_{PDMS} = 9.5%), while the fluorine block was longer. Consequently, PDMS blocks tended to aggregate as microspheres, while the surrounding regions comprised fluoride blocks, and globular pits were formed on the surface. This result agreed well with the reference that PDMS blocks in PBMA-*b*-PDMS-*b*-PBMA (f_{PDMS} < 20%) self-assembled into globular shapes on the surface [35].

As shown in Fig. 9, the samples S1, S2, S3, and S4 had different morphologies in the AFM images. It could be seen that the bright areas (yellow) in the topography images correspond to the dark areas (brown) in the phase images [8], and the hydrophobic areas are usually located as high bright spots on the surface, whereas the low dark spots are hydrophilic patches [36,37]. Therefore, the dark patches could represent the PDMS and PHFBA blocks, while the bright areas could show the PAPOSS domains in S2, S3, in the AFM topography images. By contrast, in S4, dark patches represent the PDMS blocks, and the bright areas are the PHFBA domains. As can be seen in S2 and S3, more dark areas appeared with the increased HFBA content. From the XPS results in Table 3, the silicon atomic composition in S2, S3, and S4 were similar at about 15–18%, and higher than the fluorine atomic composition, though the weight percentage of PHFBA domains increased from 38.2% to 90.5% from samples S2 to S4. Therefore, the results of AFM could be favorably compared with the XPS analysis. In addition, there appeared to be a certain degree of microphase separation in the AFM phase images, which was consistent with evidences for multiple phases provided by DSC and TEM.

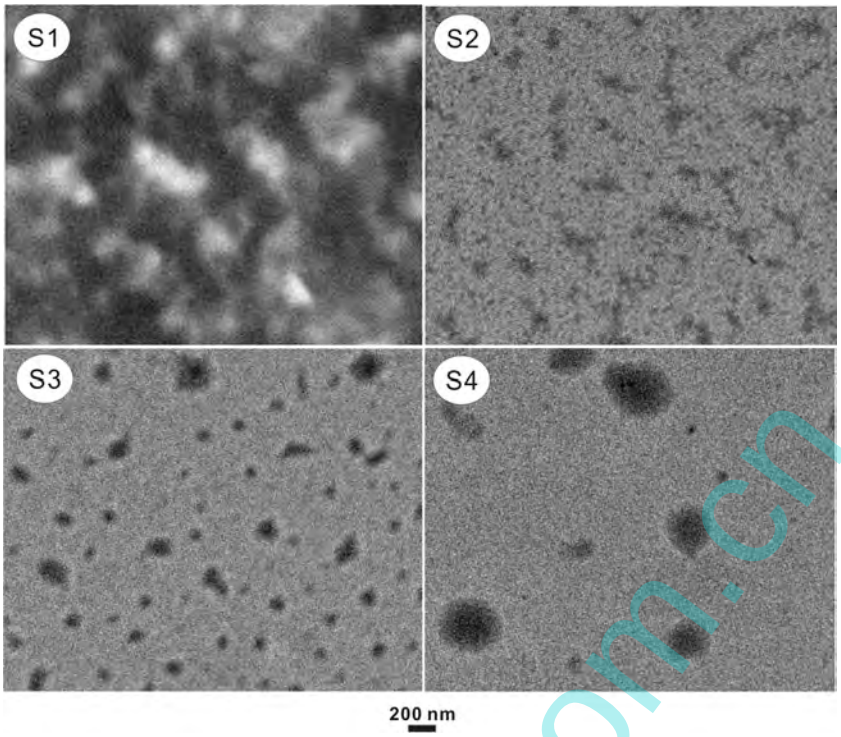

Fig. 7. TEM images of S1, S2, S3 and S4.

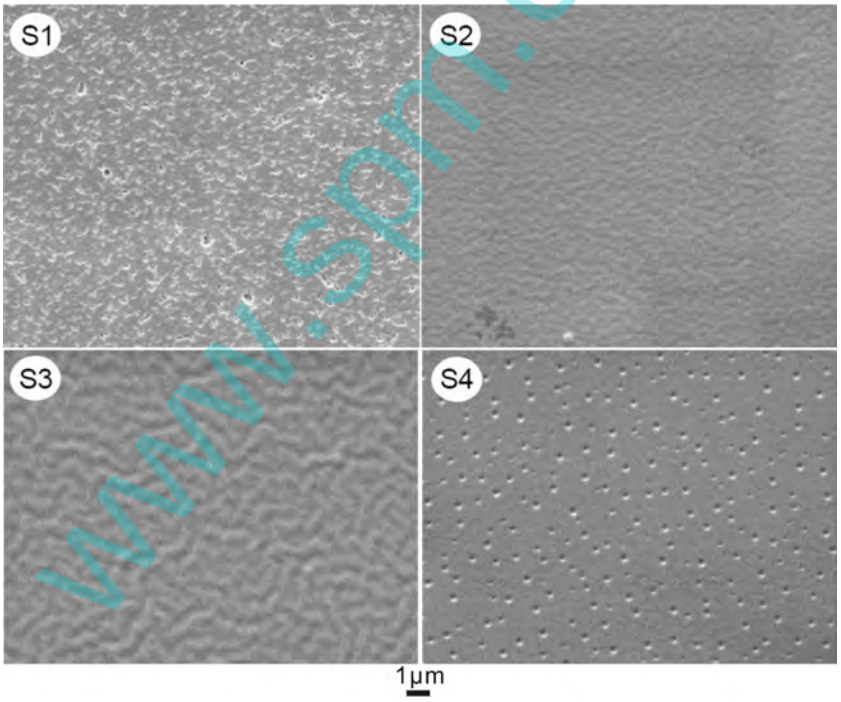

Fig. 8. SEM images of S1, S2, S3 and S4.

Table 3
Elemental composition of the copolymer surface of S2, S3 and S4 detected by XPS.

Sample	C (atomic%)	O (atomic %)	Si (atomic %)	F (atomic %)	Si/C	Si/F
S2	55.5	25.1	18.3	1.2	0.33	15.3
S3	55.9	24.8	16.6	2.8	0.30	5.9
S4	52.5	22.0	15.5	9.9	0.29	1.6

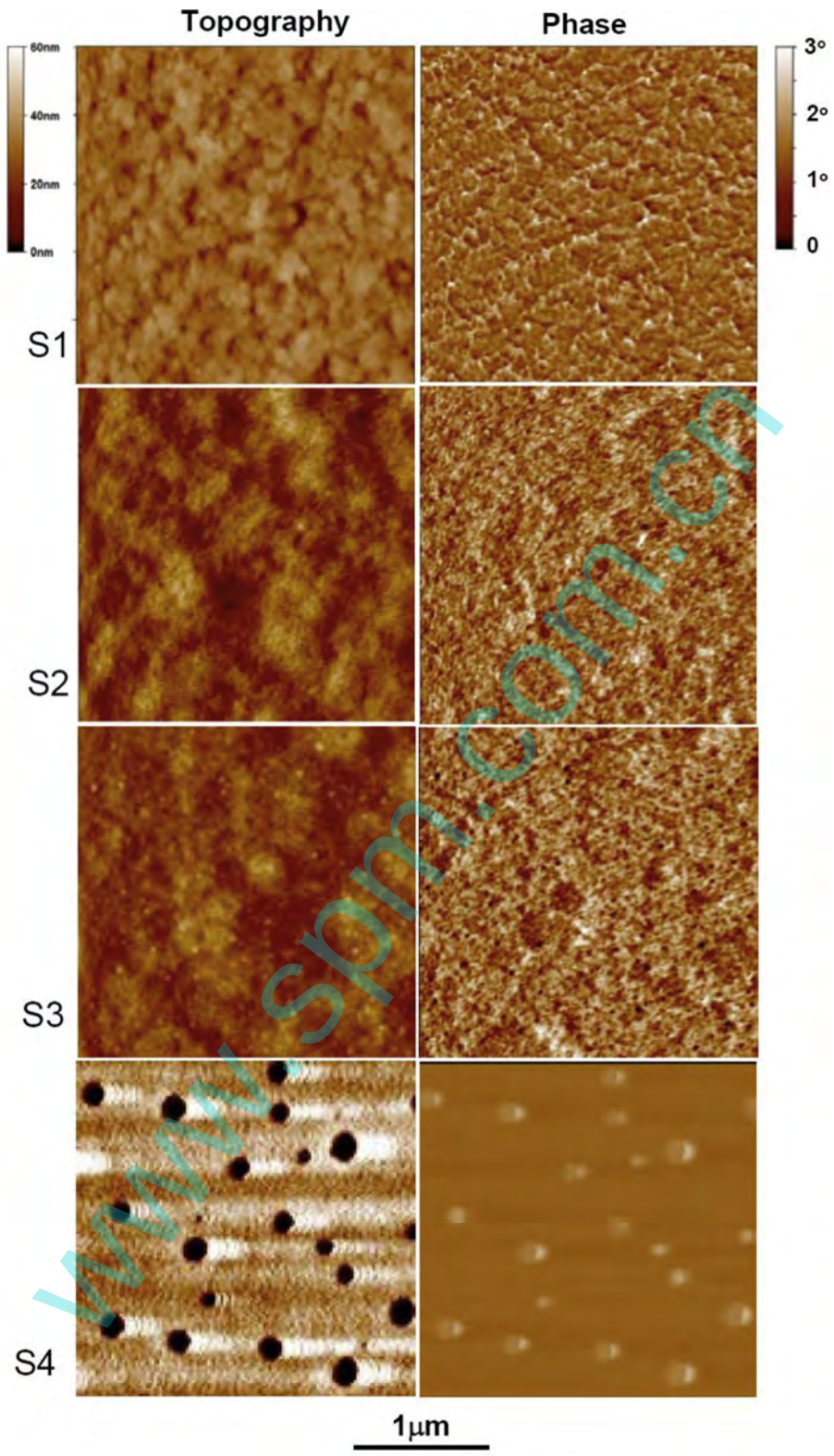

Fig. 9. AFM topography and phase images of S1, S2, S3 and S4 over a scope of 2.5 μm × 2.5 μm.

Moreover, we also obtained roughness data (R_q) from the AFM analysis as shown in Table 4, and all the average roughness values of the crosslinked films increased with the increased content of POSS. This result could be explained by the observation that the POSS units were likely to cluster in the polymer blocks and migrated to the polymer surfaces, leading to an increase in surface roughness [6].

Water contact angle measurements were carried out to analyze surface wettability. The results of these, including static water contact angles (WCA), as well as advancing (θ_a) and receding (θ_r) contact angles were also summarized in Table 4. As already known, both the surface morphology and composition of a copolymer film have influences on its WCA, θ_a, and θ_r values [1]. In these experiments, samples S2 and S3 exhibited higher WCA values than that of

Table 4
Surface properties of the copolymer films.

Sample	R_q [a] (nm)	Surface energy (mN/m)	Water contact angle (°)				Ice shear strength (kPa)
			WCA	θ_a	θ_r	θ_h	
S1	–	26.89	101.0 ± 0.9	111.8 ± 2.5	95.1 ± 0.9	16.7 ± 0.6	–
S2	1.75	25.68	106.8 ± 0.9	115.4 ± 0.7	96.4 ± 1.3	19.1 ± 1.4	385 ± 14
S3	1.10	26.09	105.1 ± 0.2	113.3 ± 3.8	73.0 ± 2.7	40.7 ± 0.6	247 ± 20
S4	1.03	25.87	102.3 ± 0.3	114.0 ± 1.0	75.4 ± 1.1	38.6 ± 0.6	276 ± 10

[a] Average roughness was measured by AFM.

S1; this was presumably due to the incorporation of the hydrophobic PHFBA blocks and crosslinking. Meanwhile, the WCA values of the samples S2 and S3 were higher than that of sample S4 because of the presence of POSS. Importantly, the water contact angle hysteresis (θ_h) values of S1 and S2 were significantly lower than those of S3 and S4 because the latter two samples had higher PHFBA weight percentages (>60%). Even for pentablock copolymers with the same structure, the sample S2, which had a higher POSS percentage, showed a significant increase in the θ_r value in comparison with that of S3. It has been suggested that the increased surface roughness generated by POSS has a more important effect on WCA than surface composition does [38,39].

From Table 4, it could also be seen that the ice shear strength of S3 had the lowest value (247 ± 20 kPa) in all the samples, though they had a similar surface energy ca. 26 mN/m. The higher content of the fluorine blocks is not suitable for anti-icing because it can enhance the interaction between the polymer surface and water [40]. Therefore, the larger content of the PHFBA block induced S4 having a higher ice shear strength (276 ± 10 kPa) than that of S3. By contrast, it has been suggested that the higher ice shear strength (385 ± 14 kPa) of S2 can be associated with its rougher surface. Overall, the ice shear strength has a direct relationship with the chemical structure and surface morphology [8]. Introducing POSS could possibly improve the anti-icing and anti-frosting properties of a polymer film by decreasing its water receding angle or its contact angle hysteresis [24], but the POSS content could simultaneously make it difficult for the block copolymers to form proper films. It was necessary to introduce PHFBA blocks so that the copolymers could be easily transferred into films, and the fluorine content could also modify the surface properties to induce low ice shear strength. Overall, the POSS-containing fluorosilicone block copolymers combined the advantages of POSS, PDMS and fluoropolymers synergistically in an appropriate way. It is intended that further studies will be undertaken to study the detailed properties of hydrophobic films with different compositions caused by well-defined POSS-containing block copolymers.

4. Conclusions

A series of POSS-containing fluorosilicone block copolymers were synthesized via RAFT polymerization by employing CTA-PDMS-CTA as the macro-chain transfer agent. Kinetic data obtained from ^{1}H NMR and GPC measurements showed that the initial chain transfer of the APOSS monomer to CTA-PDMS-CTA proceeded in a controlled way, but that the subsequential chain extension of PHFBA based on PDMS-*b*-(PAPOSS)$_2$ showed a PDI ca. 2. All the block copolymers including PDMS-*b*-(PAPOSS)$_2$ (S1), PDMS-*b*-[PAPOSS-*b*-PHFBA-*b*-P(HFBA-*co*-HEA)]$_2$ (S2 and S3), and PDMS-*b*-[PHFBA-*b*-P(HFBA-*co*-HEA)]$_2$ (S4) exhibited microphase separation morphologies evidenced by DSC, TEM, and AFM. In particular, the sample S3 with a suitable proportion of POSS and a higher PFHBA content exhibited better hydrophobic properties as determined by water contact angle measurement. It also showed lower ice shear strength than other samples of S2 and S4. Generally, block copolymers having the advantageous properties of POSS, PDMS, and fluoropolymers could have potential uses as coating materials for many applications such as anti-icing, anti-frosting, and other non-wetting technologies.

Acknowledgments

This work is financially supported by National Natural Science Foundation of China (Nos. 51273146 and 51103061) and Natural Science Foundation of Tianjin, China (No. 14ZCZDGX00008).

References

[1] N. Saleema, M. Farzaneh, R.W. Paynter, D.K. Sarkar, J. Adhes. Sci. Technol. 25 (2011) 27–40.
[2] E. Pouget, J. Tonnar, P. Lucas, P. Lacroix-Desmazes, F.O. Ganachaud, B. Boutevin, Chem. Rev. 110 (2010) 1233–1277.
[3] E. Martinelli, M.K. Sarvothaman, G. Galli, M.E. Pettitt, M.E. Callow, J.A. Callow, S.L. Conlan, A.S. Clare, A.B. Sugiharto, C. Davies, Biofouling 28 (2012) 571–582.
[4] Z.H. Luo, H.J. Yu, W. Zhang, J. Appl. Polym. Sci. 113 (2009) 4032–4041.
[5] J. Liang, L. He, X. Zhao, X. Dong, H. Luo, W. Li, J. Mater. Chem. 21 (2011) 6934–6943.
[6] S.T. Iacono, S.M. Budy, D.W. Smith, J.M. Mabry, J. Mater. Chem. 20 (2010) 2979–2984.
[7] N. Amir, A. Levina, M.S. Silverstein, J. Polym. Sci. A: Polym. Chem. 45 (2007) 4264–4275.
[8] D.M. Yu, Y.H. Zhao, H. Li, H.Z. Qi, B. Li, X.Y. Yuan, Prog. Org. Coat. 76 (2013) 1435–1444.
[9] T. Hirai, M. Leolukman, S. Jin, R. Goseki, Y. Ishida, M.A. Kakimoto, T. Hayakawa, M. Ree, P. Gopalan, Macromolecules 42 (2009) 8835–8843.
[10] B. Ahn, T. Hirai, S. Jin, Y. Rho, K.-W. Kim, M.-A. Kakimoto, P. Gopalan, T. Hayakawa, M. Ree, Macromolecules 43 (2010) 10568–10581.
[11] H. Hussain, B. Tan, K. Mya, Y. Liu, C. He, T.P. Davis, J. Polym. Sci. A: Polym. Chem. 48 (2010) 152–163.
[12] B.H. Tan, H. Hussain, C.B. He, Macromolecules 44 (2011) 622–631.
[13] J. Pyun, K. Matyjaszewski, J. Wu, G.M. Kim, S.B. Chun, P.T. Mather, Polymer 44 (2003) 2739–2750.
[14] H. Shinoda, K. Matyjaszewski, Macromol. Rapid Commun. 22 (2001) 1176–1181.
[15] D. Kessler, P. Theato, Langmuir 25 (2009) 14200–14206.
[16] K.Y. Mya, E.M.J. Lin, C.S. Gudipati, L. Shen, C. He, J. Phys. Chem. B 114 (2010) 9119–9127.
[17] W. Zhang, B. Fang, A. Walther, A.H.E. Mueller, Macromolecules 42 (2009) 2563–2569.
[18] S.M. Ramirez, Y.J. Diaz, C.M. Sahagun, M.W. Duff, O.B. Lawal, S.T. Iacono, J.M. Mabry, Polym. Chem. 4 (2013) 2230–2234.
[19] Y. Deng, J. Bernard, P. Alcouffe, J. Galy, L. Dai, J.F. Gerard, J. Polym. Sci. A: Polym. Chem. 49 (2011) 4343–4352.
[20] C. Yang, Y. Deng, B. Zeng, C. Yuan, M. Chen, W. Luo, J. Liu, Y. Xu, L. Dai, J. Polym. Sci. A: Polym. Chem. 50 (2012) 4300–4310.
[21] G. Moad, E. Rizzardo, S.H. Thang, Polymer 49 (2008) 1079–1131.
[22] R. Karunakaran, J.P. Kennedy, J. Polym. Sci. A: Polym. Chem. 45 (2007) 4284–4290.
[23] J.T. Lai, D. Filla, R. Shea, Macromolecules 35 (2002) 6754–6756.
[24] A.J. Meuler, D.J. Smith, K.K. Varanasi, J.M. Mabry, G.H. McKinley, R.E. Cohen, ACS Appl. Mater. Interfaces 2 (2010) 3100–3110.
[25] P. Kim, T.S. Wong, J. Alvarenga, M.J. Kreder, W.E. Adorno-Martinez, J. Aizenberg, ACS Nano 6 (2012) 6569–6577.
[26] A. Romo-Uribe, P. Mather, T. Haddad, J. Lichtenhan, J. Polym. Sci. B: Polym. Phys. 36 (1998) 1857–1872.
[27] L. Zheng, A.J. Waddon, R.J. Farris, E.B. Coughlin, Macromolecules 35 (2002) 2375–2379.
[28] S. Krause, M. Iskandar, M. Iqbal, Macromolecules 15 (1982) 105–111.
[29] R. Muppalla, S.K. Jewrajka, Polymer 53 (2012) 1453–1464.
[30] H. Cheng, Y.N. Zhou, Z.H. Luo, Colloids Surf. A: Physicochem. Eng. Aspects 436 (2013) 990–999.
[31] Y.C. Gan, X.S. Jiang, J. Yin, Macromolecules 45 (2012) 7520–7526.
[32] H. Yang, P.H. Pi, X.F. Wen, D.F. Zheng, Y. Cheng, Z.R. Yang, Prog. Chem. 22 (2010) 1133–1141.

[33] M.D. Rodwogin, C.S. Spanjers, C. Leighton, M.A. Hillmyer, ACS Nano 4 (2010) 725–732.
[34] J.M. Widin, A.K. Schmitt, A.L. Schmitt, K. Im, M.K. Mahanthappa, J. Am. Chem. Soc. 134 (2012) 3834–3844.
[35] H. Wang, Q. Tao, J. Wang, E. Khoshdel, Polym. Int. 60 (2011) 798–806.
[36] B.B. Sauer, R.S. McLean, R.R. Thomas, Langmuir 14 (1998) 3045–3051.
[37] H. Tan, J. Li, M. Guo, R. Du, X. Xie, Y. Zhong, Q. Fu, Polymer 46 (2005) 7230–7239.
[38] S. Pal, H. Weiss, H. Keller, F. Müller-Plathe, Langmuir 21 (2005) 3699–3709.
[39] S.T. Iacono, S.M. Budy, J.M. Mabry, D.W. Smith, Macromolecules 40 (2007) 9517–9522.
[40] H. Murase, K. Nanishi, H. Kogure, T. Fujibayashi, K. Tamura, N. Haruta, J. Appl. Polym. Sci. 54 (1994) 2051–2062.